

See discussions, stats, and author profiles for this publication at: <https://www.researchgate.net/publication/263943504>

Coal Swelling Model for Pressurized High Particle Heating Rate Pyrolysis Applications

ARTICLE *in* ENERGY & FUELS · MAY 2012

Impact Factor: 2.79 · DOI: 10.1021/ef300442r

CITATIONS

11

READS

28

5 AUTHORS, INCLUDING:



[Thomas H. Fletcher](#)

Brigham Young University - Provo Main Campus

155 PUBLICATIONS 2,290 CITATIONS

[SEE PROFILE](#)

Coal Swelling Model for Pressurized High Particle Heating Rate Pyrolysis Applications

Randy C. Shurtz, Joseph W. Hogge, Kade C. Fowers, Gregory S. Sorensen, and Thomas H. Fletcher*

Department of Chemical Engineering, Brigham Young University, Provo, Utah 84602, United States

ABSTRACT: A model was previously developed to describe the decrease in swelling during coal pyrolysis at atmospheric pressure when maximum particle heating rates increase from 10^4 K/s to 10^5 K/s. That model included effects of coal type using chemical structure properties. This paper presents results of new experiments to study the effects of elevated pressure and high heating rates on coal pyrolysis. A pressurized flat-flame burner (PFFB) was designed and built to conduct these studies. The pyrolysis experiments reported in this paper were conducted at particle heating rates of $\sim 10^5$ K/s and maximum gas temperatures of 1700 to 1900 K at pressures of 1 to 15 atm. Residence times of 25–85 ms were used. A new coal swelling correlation was developed that predicts the effects of heating rate, pressure, and coal rank on the swelling ratio at heating rates above $\sim 10^4$ K/s. The coal rank index parameters from a previously published atmospheric swelling model were used to model the pressurized swelling data, and a new correlation was developed to describe the effects of pressure. The resulting empirical correlation fits pressurized swelling data from a wide range of coals and types of reactors that could not previously be explained by any one model.

1. INTRODUCTION

As coal particles are heated, a distribution of volatile species with a distribution of molecular weights are released into the gas phase. Volatile gases that condense at room temperature and pressure are termed tars, and noncondensable gases are termed light gases. For softening coals at higher pressures, vaporization of the tar is inhibited; only the very lightest molecules have a high enough vapor pressure to leave the particle. This decreases the yield of tar. The retained tar precursors (i.e., Metaplast) are cross-linked back into the polymer network to become part of the char. Aliphatic attachments from molecules that remain in the Metaplast increase the yield of light gases. The net effect of higher pyrolysis pressure is to decrease the total yield of volatiles and decrease the average molecular weight of the tar.¹ The effect of total pressure on pyrolysis yield has been captured in network pyrolysis models by treating tar vaporization as a flash-distillation process.

At elevated pressures, the Metaplast is enriched in lighter molecules, which act as plasticizers, enhancing bubble growth. Greater swelling and higher porosity have been observed at elevated pressures because bubbles are able to grow to larger sizes without popping.^{2,3} Group I chars (or Cenospheres) have been found to be more prevalent.^{2,4} However, swelling cannot increase without bound as pressure increases. Very high external pressures are better able to counteract the lower pressure generated inside the bubbles due to lower volatiles release. A recent model includes the competition of these two effects of increasing pressure and predicts that the swelling ratio decreases slowly as total pressure increases beyond 8–10 atm (Figure 1).⁵

The coal swelling ratio or swelling parameter is defined for pulverized coal as the char particle diameter after pyrolysis divided by the initial coal particle diameter. The swelling ratio is the simplest and perhaps the most useful measure of char

structure. The initial char particle diameter is a critical parameter for practically all combustion and gasification models, regardless of the level of sophistication.

A simple example of the effect of particle size on gasification rates is shown in Figure 2. These conversion profiles were estimated using first-order Illinois #6 rate parameters from the literature.⁷ Coal particles with diameters of 50 μm and 14% postpyrolysis dry ash content were assumed. A constant gas temperature of 1700 K was specified at 15 atm with surroundings at 1000 K and 20 mol % CO₂ in the bulk gas. A mode-of-burning parameter of 0.2 was specified, as has been recommended for combustion modeling.⁸ A more sophisticated model would predict rates that decrease more with increasing residence time due to nonisothermal conditions, ash inhibition, and thermal deactivation. The relationship between the predicted rate and particle diameter is more complex when effectiveness factors are used. Figure 2 shows that gasification rates and conversion times are highly sensitive to the swelling ratio. This first-order model predicts faster reaction rates for highly swollen particles because the particle has increased external surface area, even though the mass flux in the particle boundary layer is lower.

When swelling data obtained in a pressurized drop-tube furnace at 10^4 K/s³ are compared to data from facilities that enhance the particle heating rates using O₂,² or flat-flame burners,⁶ as in Figure 1, it becomes apparent that the effect of heating rate on coal swelling is very important for pyrolysis at elevated pressures. The maximum reported swelling ratio for Illinois #6 is more than twice as high at 10^4 K/s compared to that at 10^5 K/s.

Received: March 12, 2012

Revised: May 11, 2012

Published: May 18, 2012

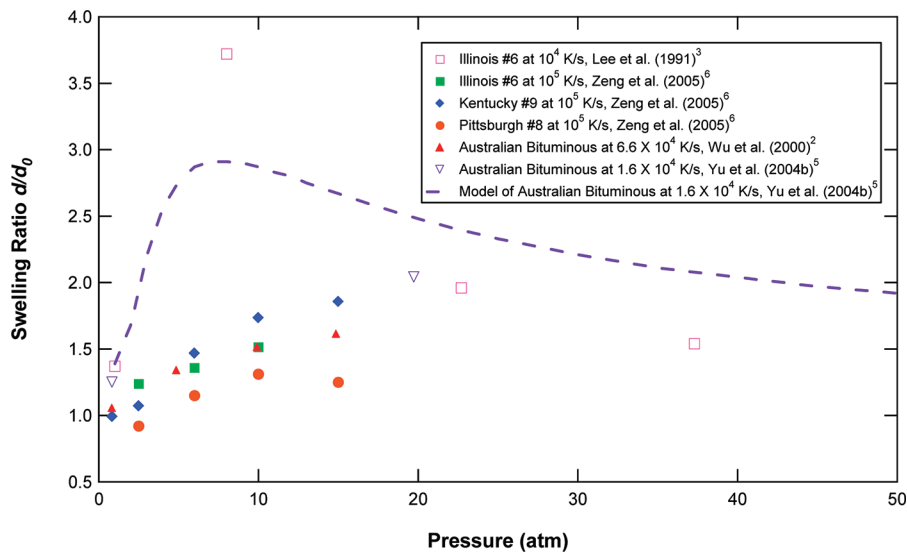


Figure 1. Swelling ratio versus pressure from pulverized coal experiments and a model.^{2,3,5,6}

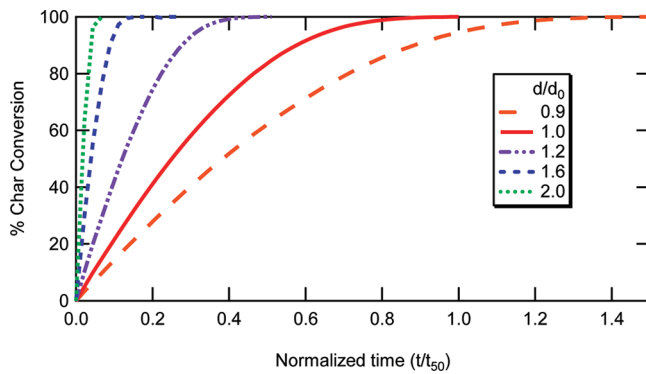


Figure 2. Calculated conversion profiles for Illinois #6 coal char gasification at different swelling ratios ($T_g = 1700$ K, $P = 15$ atm, 20% CO_2). Residence times are normalized to the 100% conversion time for a $50\ \mu\text{m}$ particle with no swelling (t_{50}).

Studies with modified drop-tube furnaces and flat-flame burners at atmospheric pressure have shown that the bituminous coal swelling ratios may decrease from greater than 1.5 at heating rates of 10^4 K/s to less than 1.05 at initial heating rates on the order of 10^5 K/s.^{9–11} This decrease in swelling at high heating rates has been attributed to a characteristic devolatilization time that is shorter than the characteristic relaxation time of the viscous coal melt. The bubbles burst at very high heating rates, followed by cross-linking.

The most advanced swelling models based on the physics of bubble formation predict increased swelling with increasing heating rate, but they fail to predict decreased swelling at heating rates above 10^4 K/s.^{5,12} There is some indication that different formulations may allow mechanistic models to predict decreased swelling with increasing heating rate,^{13,14} at least on a qualitative level. Advanced swelling models^{5,12} are inconvenient

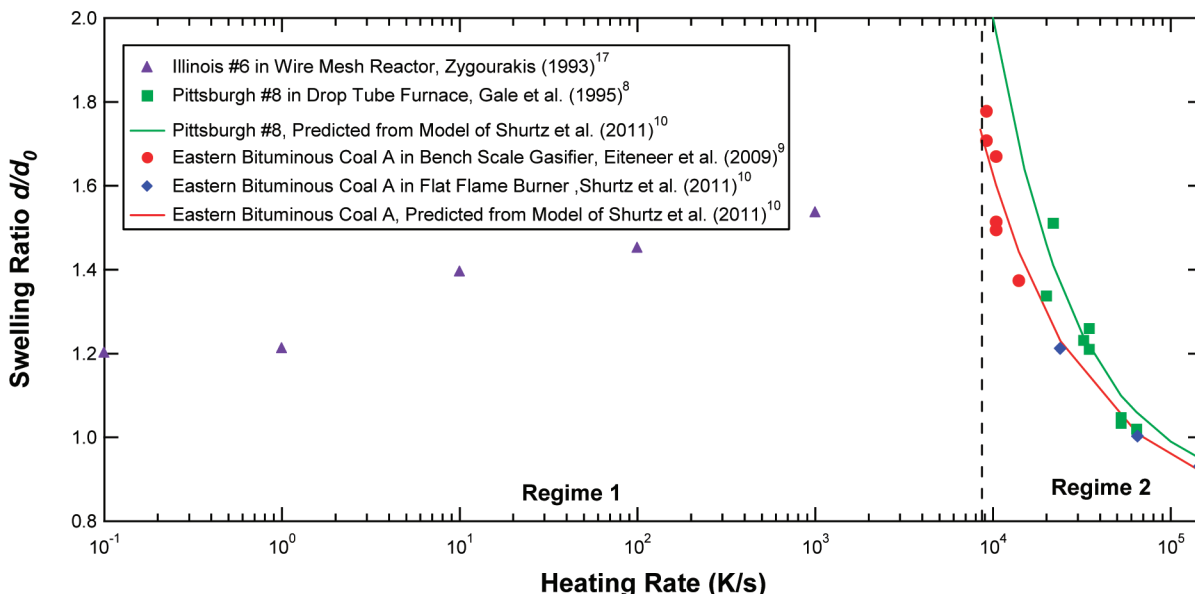


Figure 3. Measured and predicted atmospheric swelling during coal pyrolysis as a function of heating rate, denoting regimes of increasing/decreasing swelling.^{9–11,18}

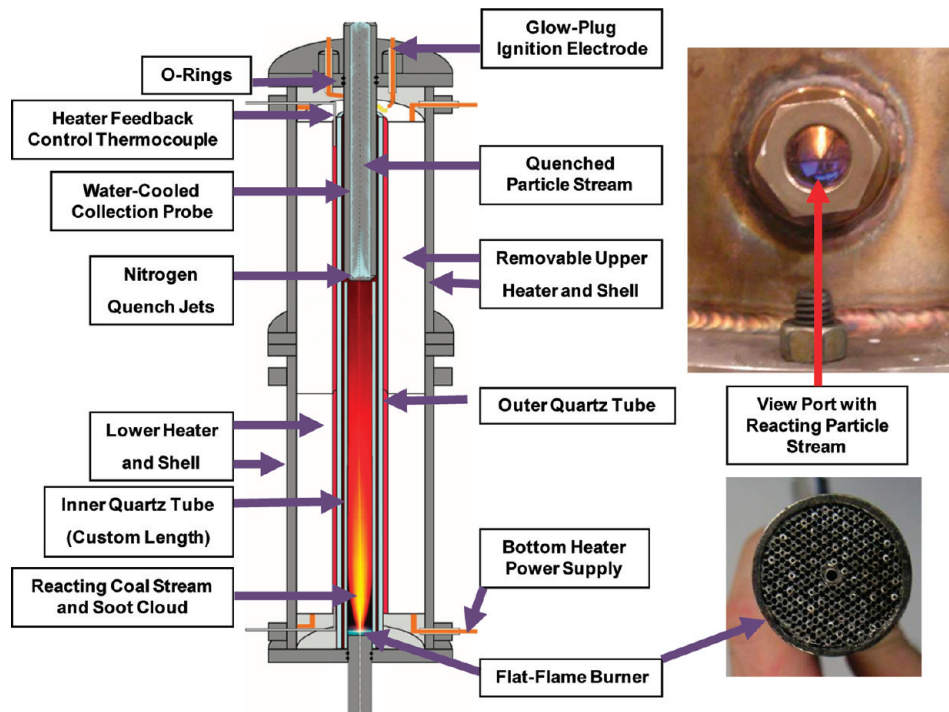


Figure 4. PFFB cross-section illustration (left), burner face (bottom right), and operating burner (top right). Figure taken from Shurtz.¹⁹

for most practical applications because the computational cost is high and input parameters can be difficult to obtain. It is extremely difficult to measure physical properties such as viscosity in reacting Metaplast. Other detailed inputs such as density distributions are inconvenient to measure. Most existing empirical swelling models also fail to properly capture the effect of heating rate.^{15–17} An empirical correlation for coal particle swelling during high heating rate pyrolysis at atmospheric pressure was recently published.¹¹ Coal rank effects were included in the correlation based on parameters representing the chemical structure of the coal. The form of the proposed correlation allowed prediction of decreased swelling behavior for bituminous coals observed between 10^4 and 10^5 K/s (denoted as regime 2 in Figure 3).

The work presented in this paper includes results of additional coal pyrolysis experiments performed in a pressurized flat-flame burner to achieve particle heating rates of 10^5 K/s at pressures up to 15 atm and gas temperatures up to 1700 K. The swelling data obtained were used to develop a modification to the high heating rate swelling correlation of Shurtz et al.¹¹ that accounts for the effects of pressure.

2. EXPERIMENTAL SECTION

A newly developed pressurized flat-flame burner (PFFB) system was used to perform the pyrolysis tests at pressures up to 15 atm. A schematic of the PFFB system is shown in Figure 4 and is fully described by Shurtz.¹⁹ The flat-flame burner consisted of an array of tubes that delivered a gaseous fuel to a surface, while an oxidizer-rich gas was fed through the honeycomb spaces between the tubes. A glow plug made from a thermocouple wire was used as the ignition device. The resulting flat flame was ~1 mm thick. The burner diameter was 1 in. (2.5 cm), and the inner diameter of the pressure vessel was 6 in. (15.2 cm).

Coal particles were entrained in a stream of N₂ and fed through a larger tube at the center of the array, with particle feed rates of ~1 g/h or less to ensure single-particle behavior. Coal particles were heated convectively by the postflame gases at heating rates on the order of 10^5

K/s for particles smaller than ~100 μ m. These particle heating rates are 2–10 times higher than conventional electrically heated drop-tube furnaces.

The postflame gases in the PFFB flowed through a quartz tube where reactions with coal took place. Insulation was placed between the quartz tube and the pressure vessel to reduce heat loss. A water-cooled collection probe was located at the end of the quartz reaction tube to quench the hot gases and particles with jets of N₂. The interior liner of the collection probe consisted of a sintered metal tube through which additional N₂ was passed in order to eliminate tar and soot deposition in the probe. The collection probe could be moved up and down on a track system to adjust residence time (up to 800 ms). The burner also had a more limited range of motion that allowed for residence times as low as 30 ms, corresponding to particle collection heights of less than 1 in.

A schematic of the particle collection system is shown in Figure 5. The collection system is similar to that used by Zeng,^{6,20} consisting of a virtual impactor, cyclone, and filter system. The 50% cut point diameter on the virtual impactor and cyclone was 5 μ m. Care was taken to slowly depressurize the cyclone chamber so that char particles were not shattered due to high velocity flows (see Shurtz¹⁹).

Char and soot were collected and analyzed separately. Details regarding soot collection and analysis are reported elsewhere.¹⁹ The average change in particle mass was determined by a direct mass balance and also by an ash tracer technique. Similar experiments were performed in an existing atmospheric flat-flame burner (FFB) facility^{21,22} to allow comparison to the previously published atmospheric swelling model.¹¹

The average change in particle size was calculated from the measured changes in mass and bulk density, with the assumption that the particle shape did not change enough to alter the packing factor. The tap technique was used to determine bulk densities of all coals and chars.^{9,23,24} The swelling ratio was determined using the following relationship:

$$\frac{d}{d_0} = \left(\frac{m/m_0}{\rho/\rho_0} \right)^{1/3} = \left(\frac{[m/m_0]}{\left[\frac{\rho_b}{1 - \epsilon_b} \right] \left[\frac{1 - \epsilon_{b0}}{\rho_{b0}} \right]} \right)^{1/3} \quad (1)$$

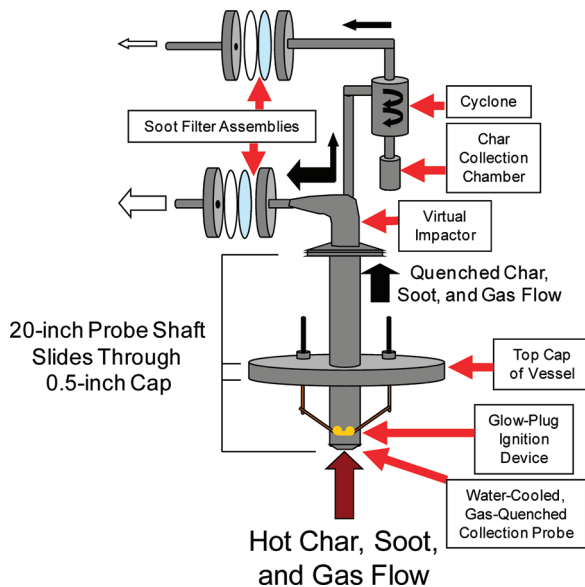


Figure 5. Collection probe with aerodynamic separation system for char and soot collection.

where the terms with the subscript 0 refer to the parent coal and the other terms refer to the char. The residual mass ratio m/m_0 in this equation is expressed on an as-received basis. The density ratio ρ/ρ_0 refers to the ratio of apparent densities, where apparent density is defined as the mass of a particle divided by the total volume enclosed by the outer surface of the particle (assumed to be spherical). With this assumption, the packing factors canceled out and the bulk densities were used directly to determine the swelling ratio. The error associated with this method has been estimated to be 10%.²⁴

Initial pressurized pyrolysis experiments were conducted in fuel-rich CO flames in the pressurized flat-flame burner (PFFB) to provide information needed for gasification studies, especially char particle size. CO was used instead of CH₄ or other hydrocarbons because of the strong sooting tendencies of the hydrocarbon gases at elevated pressures. Unfortunately, fragmentation of the char and contamination of the char with very large soot agglomerates were prevalent when these experiments were conducted, especially at elevated pressure (see Shurtz¹⁹). A density separation procedure in an ethanol–water mixture was developed in an attempt to fix these problems, but was not able to fully separate the soot from the char. Due to the lower tar yield and lack of swelling behavior, the Wyodak subbituminous coal studied was not strongly influenced by soot contamination and fragmentation (see Figure 6), so it was not subjected to the separation procedure.

Additional pyrolysis experiments with 2 mol % O₂ and a vertical cyclone yielded intact char particles with little soot. The residence times were short enough for oxidation of the char to be negligible. At the conditions used in this study and in pulverized coal boilers and gasifiers, the effect of ambient gas composition on swelling is probably very small because the blowing effect during rapid pyrolysis inhibits

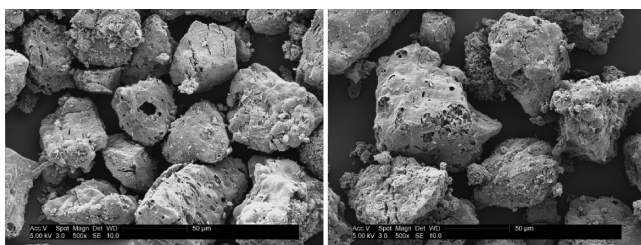


Figure 6. Wyodak chars produced at 2.5 atm, 33 ms (left) and 15 atm, 44 ms (right).

transport of surrounding gases to the surface of pyrolyzing coal particles.²³ The swelling ratios were evaluated on a raw basis, without the use of the density separation technique in a liquid. The quality of the char density measurements was checked by vibrating the chars in argon overnight. The stratified char sample was checked for the presence of a dark, sooty layer, and the char bed was then remixed to remove the stratification effects. If there were large differences in the bulk density of the char before and after vibration, it was taken as an indicator of soot in the raw char. SEM images were used to verify the presence or lack of soot in each char sample and to determine whether the previbration or postvibration densities were most suitable for swelling ratio calculations.

The soot layer that was sometimes present in the vibrated char was very thin and occurred at the bottom of the glass vial. This differed from previous observations of atmospheric chars with shorter vibration times.²⁵ It is thought that the prolonged vibration time caused the soot agglomerates to become denser. Very dense soot agglomerates were observed by SEM in some of the vibrated chars.

The properties of the coals studied in this work are listed in Table 1. The NMR parameters in Table 1 are defined in Table 2 and were predicted using correlations with the ultimate and proximate analyses²⁶ (see Shurtz¹⁹). The correlated parameter c_0 is also used in the CPD model²⁷ to represent stable biaryl linkages in very high rank coals and low-temperature cross-linking in low rank coals.

Gas temperatures were measured with a B-type thermocouple and corrected for radiation effects on the thermocouple junction.¹⁹ Residence times were determined from particle velocities, which were measured optically with a high-speed camera.¹⁹ The particle temperature history was determined from an energy balance using a 1-D code that includes the CPD model.^{26–28} CPD model predictions indicate that the chars were fully pyrolyzed at the experimental residence times of 26 to 83 ms. Residence times were higher at the higher pressures, and were typically above 65 ms for the O₂-rich pressurized pyrolysis conditions. Completion of pyrolysis was also verified in scoping experiments that showed negligible incremental mass loss with further increases in residence time. Typical differences between raw temperature measurements, radiation-corrected temperatures, and predicted particle temperatures are shown in Figure 7. The predicted temperatures in Figure 7 were produced using a spherical thermocouple bead junction with a diameter of 373 μm , an initial coal particle diameter of 63 μm , and surroundings with an average temperature of 500 K.

3. RESULTS

The mass release, density, and residence time data are presented in Table 3, along with the derived swelling ratios. In most cases, the ash tracer technique gave more reasonable mass release than the direct mass balance when compared to the ASTM volatile matter. The direct mass balance appeared more reasonable for some of the bituminous coals at low pressure (see Table 3). It is thought that the direct mass balance yielded higher mass release due to the small amount of sample fed and perhaps imperfect capture of the most highly swollen char particles in the PFFB. The mass release either stayed fairly constant or decreased slightly with increasing pressure. Decreasing volatiles yield with increasing pressure has been attributed to the vapor pressure effect.¹ The measured volatiles yields at 5 atm appear to be less consistent in terms of the overall trends.

The swelling ratios are compared for the different coals in Figure 8. With the exception of Pittsburgh #8, the bituminous swelling ratios in Figure 8 are largest at pressure near 10 atm. The swelling ratios are all lower than 2, which is consistent with measurements made at heating rates near 10⁵ K/s in previous studies, but lower than measurements made near 10⁴ K/s (see Figure 1). The subbituminous coals exhibited little if any swelling, which was consistent with the SEM images (see

Table 1. Properties of Coals Studied in This Work

	Wyodak	Dietz	Adaville #1	Kentucky #9
particle size (μm , from mesh)	45–75	63–75	53–63	45–75
mass mean size (μm)	67	74	46	58
C (mass % daf)	68.83	68.48	70.64	77.01
H (mass % daf)	5.59	5.37	5.32	5.61
N (mass % daf)	0.94	0.86	1.03	1.69
S (mass % daf)	0.53	0.48	1.03	4.00
O (mass % daf, by diff.)	24.12	24.81	21.98	11.69
VM (mass % daf)	53.61	44.64	44.57	46.27
ash (mass % dry)	5.63	4.83	3.33	8.07
moisture (mass % as received)	dried to 5.7	17.71	13.66	1.84
apparent particle density (g/cm^3)	1.23	1.25	1.33	1.21
M_δ	49.7	49.7	47.2	40.1
MW	398.9	388.6	381.0	416.1
p_0	0.547	0.591	0.567	0.445
$\sigma+1$	4.38	4.38	4.63	5.18
c_0	0.150	0.150	0.133	0
	Illinois #6	Pittsburgh #8	Lower Kittanning	
particle size (μm , from mesh)	53 to 66	45–75 ^a	63–75	
mass mean size (μm)	68	37 ^a	74	
C (mass % daf)	76.68	82.19	86.38	
H (mass % daf)	5.54	5.42	4.84	
N (mass % daf)	1.45	1.58	1.59	
S (mass % daf)	3.60	2.23	2.53	
O (mass % daf, by diff.)	12.73	8.58	4.66	
VM (mass % daf)	42.27	38.80	21.64	
ash (mass % dry)	8.46	6.57	17.56	
moisture (mass % as received)	7.53	1.21	0.71	
apparent particle density (g/cm^3)	1.21	1.28	1.39	
M_δ	40.5	31.9	21.3	
MW	408.8	360.7	297.7	
p_0	0.471	0.508	0.662	
$\sigma+1$	5.12	5.08	4.88	
c_0	0.003	0	0.059	

^aThe mesh size was listed on the bottle, but the Coulter Counter results show a lot of material <45 μm .

Table 2. Structural Parameter Definitions Derived from ^{13}C NMR spectroscopy measurements

structural param.	description
$\sigma+1$	coordination no.; avg no. of attachments per aromatic cluster
p_0	fraction of attachments that are intact loops or bridges
M_δ	avg molecular weight of an attachment
MW	avg aromatic cluster molecular weight, including associated attachments

Figure 6). The lack of swelling for subbituminous coals can be attributed to low-temperature cross-linking, which results in a lack of fluidity in the Metaplast and lower tar yields compared to bituminous coals. This early cross-linking is generally attributed to higher oxygen content in the coal.²⁹

SEM images of some of the bituminous chars produced in the PFFB are shown in Figure 9. The 15 atm chars are larger and internal bubble structure is more evident compared to the

5 atm chars because the 15 atm particles have thinner walls. All of the bituminous coals exhibited greater changes in structure and size compared to the subbituminous coals (see Figure 6), which released volatile products through their existing pore structures rather than through bubbles.

The Adaville #1 was selected for follow-up pyrolysis experiments to test the performance of the pressurized swelling correlation, which was developed from the other coals studied in this work. The rank of the Adaville #1 coal is near the transition between subbituminous and bituminous, which suggests that its pyrolysis swelling behavior should be difficult to predict with accuracy. As expected, the extent of swelling observed for Adaville #1 was higher than the subbituminous coals studied, but much lower than the other bituminous coals. Since the rank of the Adaville #1 coal occurs where steep gradients in swelling behavior versus coal rank are expected, the data from this coal allow the model performance to be evaluated under a worst-case scenario.

4. DISCUSSION

In previous work, the swelling ratio was found to correlate well with the maximum derivative of particle temperature with respect to residence time, assuming lumped capacitance:^{9,11,23}

$$\dot{T} = \left(\frac{dT_p}{dt} \right)_{\max} \quad (2)$$

This is the heating rate that was used to develop the previous atmospheric pressure swelling correlation for particles smaller than $\sim 200 \mu\text{m}$.¹¹ Since the heating rate is somewhat sensitive to the calculation method, a standard procedure is recommended for use with this model. A particle energy balance with transient, convection, radiation, and reaction/vaporization terms was used to calculate the particle temperature history and hence the maximum particle heating rate:^{19,30}

$$m_p c_p \frac{dT_p}{dt} = \theta h A_p (T_g - T_p) - \sigma \epsilon_p A_p (T_p^4 - T_{\text{surr}}^4) - \frac{dm}{dt} \Delta H \quad (3)$$

where the terms on the right-hand side represent convection, radiation, and the heat of reaction, respectively. All symbols are defined in the nomenclature. The blowing parameter θ is defined by

$$\theta = \frac{B}{e^B - 1} \quad (4)$$

and accounts for the effects of high mass transfer. The mass flux term B in the blowing parameter is calculated for spherical particles at low Reynolds numbers as^{30–32}

$$B = \frac{-\frac{dm}{dt} \hat{\rho}_{pg}}{2\pi d_p k_g} \quad (5)$$

The CPD model was used to calculate devolatilization rates in a 1-D code.^{26–28} The Merrick heat capacity³³ was calculated at the initial temperature (300 K) and then held constant to be consistent with experimental temperature measurements at high particle heating rates.³⁴ It has been found that this procedure yields better predictions of devolatilization behavior for different particle sizes compared to using a heat capacity that varies with temperature.^{11,19} The mass-mean particle

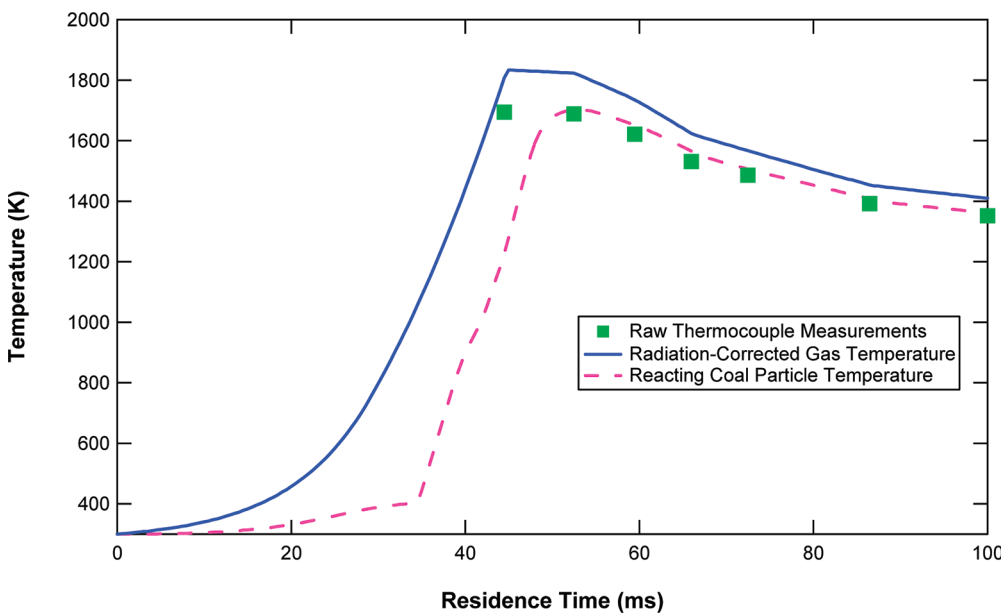


Figure 7. Temperatures for Dietz coal pyrolysis in the PFFB at 15 atm.

diameter (measured with a Coulter Counter) was used in this study. As a convention for entrained-flow reactors such as drop-tube furnaces and the flat-flame burners used in this study, the initial gas temperature at the injection point was set to 300 K, and the first elevated gas temperature was measured at a distance 10 mm to 13 mm above the burner surface. Gas temperatures were interpolated versus distance in a linear fashion for use in the energy balance. At distances closer to the injector than ~10 mm, the large gas-phase temperature gradients make thermocouple measurements highly sensitive to very small deviations in position.

In the previous correlation at atmospheric pressure,¹¹ it was found that the maximum particle heating rate occurred before the onset of devolatilization when these conventions were used in the energy balance. This allowed the swelling ratio to be predicted and applied without iteration. However, pyrolysis calculations for conditions in the PFFB indicated that the global maximum heating rate occurred at high extents of devolatilization at elevated pressures (see Figure 10). When calculations were performed for Illinois #6 coal, swelling caused an increase in convective heat transfer, which caused a slight increase in the maximum particle heating rate. The particle temperature and devolatilization rate consequently increased compared to the nonswelling case (see Figure 10).

Swelling was applied linearly with the extent of devolatilization³⁵ in the development of this model. This approach is sufficient for most models of utility boilers and gasifiers because swelling is low and devolatilization is fast at ~10⁶ K/s. In the CPD model, there is a parameter \mathcal{L} that represents the labile bridge fraction in the polymer network.²⁷ During devolatilization calculations, the labile bridges are converted to reactive intermediates \mathcal{L}^* that can either cleave into two side chains or react to form stabilized char bridges and light gases. As the labile bridge fraction decreases from its initial value \mathcal{L}_0 to zero, the polymer network of the coal is converted to a highly cross-linked char structure, which would tend to limit swelling. Therefore, in the 1-D CPD-based code used in this work,²⁸ the labile bridge fraction was treated as a measure of the extent of

pyrolysis. The particle diameter was varied using the following equation:

$$d_p = d_{p0}(1 + \text{swell}[1 - \mathcal{L}/\mathcal{L}_0]) \quad (6)$$

where swell is the fractional swelling that is related to the experimental or model swelling ratio by swell = $(d - d_0)/d_0 = d/d_0 - 1$.

Figure 10 shows that when the swelling ratio is calculated from the model developed in this study, the temperature history predicted when the experimental swelling ratio is used as an input can be reproduced with good accuracy. The swelling ratio was recalculated each time a local maximum heating rate greater than the previous maximum particle heating rate was found. This technique resulted in a final swelling ratio, a maximum heating rate, and a volatiles yield that were consistent with the values obtained when the experimental swelling ratio was used as an input (see Figure 10) and also with the values obtained by iterating the entire calculation three or more times.

A small initial peak in the heating rate typically occurs immediately before water begins to vaporize, followed by a true maximum heating rate after water vaporization is complete (see Figure 10). The moisture content should be checked at the time corresponding to each local maximum in heating rate to ensure that the correct heating rate is used for this swelling model.

The previously developed correlation¹¹ did not account for effects of pressure on swelling during pyrolysis. In this work, a pressure-dependent term $f(P)$ was introduced into the previous correlation. The form of the pressurized swelling model is

$$\left(\frac{d}{d_0} \right)_{\text{HHR}} = s_{\text{var}} \left(\frac{\dot{T}_{\text{Base}}}{\dot{T}} \right)^{c_{\text{HR}}} f(P) + s_{\text{min}} \quad (7)$$

$$s_{\text{min}} = (\text{FC}_{\text{ASTM}} + A_{\text{ASTM}})^{1/3} \quad (8)$$

where FC_{ASTM} is the ASTM fixed carbon fraction and A_{ASTM} is the ASTM ash fraction on a dry basis. The parameter s_{min} represents the theoretical lower limit of swelling at infinitely high heating rates, assuming that the apparent particle density is constant and the trends in the volatiles yield with coal rank are

Table 3. Pyrolysis Data for Coals

Wyodak pyrolysis data with 0% O ₂								
pressure (atm)	peak gas temp. (K)	collection height (in.)	residence time (ms)	mass release (daf wt %, ash tracer)	mass release (as rec'd wt %, direct)	ash (dry wt %)	apparent density ρ (g/cm ³)	swelling ratio d/d ₀
15	1681	0.75	46	46.12	N/A	9.95	0.796	0.931
10	1722	0.75	42	44.50	N/A	9.69	0.766	0.952
5	1702	0.75	38	46.61	54.96	10.03	0.701	0.969
2.5	1683	0.75	33	46.83	56.48	10.07	0.702	0.967
pressure (atm)	2.5			5		10		15
heating rate (K/s)	7.36×10^4			7.28×10^4		6.91×10^4		6.26×10^4
Dietz pyrolysis data with ~2% O ₂								
pressure (atm)	peak gas temp. (K)	collection height (in.)	residence time (ms)	mass release (daf wt %, ash tracer)	mass release (as rec'd wt %, direct)	ash (dry wt %)	apparent density ρ (g/cm ³)	swelling ratio d/d ₀
15	1834	1.5	83	66.34	84.04	13.10	0.298	1.075
10	1907	1.5	78	53.96	74.40	9.93	0.430	1.056
5	1798	1.5	65	67.24	84.18	13.41	0.302	1.058
0.84 ^a	1662	2	26	44.66	62.72	8.40	0.546	0.948
pressure (atm)	0.84			5		10		15
heating rate (K/s)	1.64×10^5			9.53×10^4		1.05×10^5		9.58×10^4
Adaville #1 pyrolysis data with ~2% O ₂								
pressure (atm)	peak gas temp. (K)	collection height (in.)	residence time (ms)	mass release (daf wt %, ash tracer)	mass release (as rec'd wt %, direct)	ash (dry wt %)	apparent density ρ (g/cm ³)	swelling ratio d/d ₀
15	1834	1.5	83	63.74	65.95	8.67	0.251	1.205
10	1907	1.5	78	56.74	63.27	7.27	0.275	1.240
0.84 ^a	1662	2	26	48.51	64.20	6.27	0.459	1.098
pressure (atm)	0.84			10				15
heating rate (K/s)	1.89×10^5			1.34×10^5				1.18×10^5
Illinois #6 pyrolysis data with ~2% O ₂								
pressure (atm)	peak gas temp. (K)	collection height (in.)	residence time (ms)	mass release (daf wt %, ash tracer)	mass release (as rec'd wt %, direct)	ash (dry wt %)	apparent density ρ (g/cm ³)	swelling ratio d/d ₀
15	1834	1.5	83	47.32	59.32	15.02	0.129	1.699
10	1907	1.5	78	47.34	54.59	14.93	0.113	1.776
5	1798	1.5	65	47.48	66.27	15.06	0.264	1.337
0.84 ^a	1662	2	26	52.16	54.91	16.29	0.506	1.024
pressure (atm)	0.84			5		10		15
heating rate (K/s)	1.54×10^4			1.18×10^5		1.59×10^5		1.37×10^5
Kentucky #9 pyrolysis data with ~2% O ₂								
pressure (atm)	peak gas temp. (K)	collection height (in.)	residence time (ms)	mass release (daf wt %, ash tracer)	mass release (as rec'd wt %, direct)	ash (dry wt %)	apparent density ρ (g/cm ³)	swelling ratio d/d ₀
15	1834	1.5	83	44.84	55.66	13.73	0.137	1.721
10	1907	1.5	78	45.21	55.32	13.81	0.123	1.782
5	1798	1.5	65	52.89	N/A	15.71	0.108	1.784
0.84 ^a	1662	2	26	57.04	11.60	16.97	0.650	0.955
pressure (atm)	0.84			5		10		15
heating rate (K/s)	1.51×10^5			1.21×10^5		1.42×10^5		1.24×10^5
Pittsburgh #8 pyrolysis data with ~2% O ₂								
pressure (atm)	peak gas temp. (K)	collection height (in.)	residence time (ms)	mass release (daf wt %, ash tracer)	mass release (as rec'd wt %, direct)	ash (dry wt %)	apparent density ρ (g/cm ³)	swelling ratio d/d ₀
15	1834	1.5	83	44.05	60.94	11.16	0.120	1.835
10	1907	1.5	78	45.64	66.57	11.45	0.130	1.772
5	1798	1.5	65	43.75	66.67	11.11	0.143	1.732
0.84 ^b	1662	2	26	50.56	56.85		0.652	0.974
pressure (atm)	0.84			5		10		15
heating rate (K/s)	2.24×10^5			9.84×10^4		1.17×10^5		1.01×10^5
Lower Kittanning pyrolysis data with ~2% O ₂								
pressure (atm)	peak gas temp. (K)	collection height (in.)	residence time (ms)	mass release (daf wt %, ash tracer)	mass release (as rec'd wt %, direct)	ash (dry wt %)	apparent density ρ (g/cm ³)	swelling ratio d/d ₀
15	1834	1.5	83	31.92	56.36	24.11	0.142	1.829
10	1907	1.5	78	32.53	N/A	24.00	0.125	1.900
5	1798	1.5	65	11.83	38.30 ^c	19.46	0.203	1.615
0.84 ^a	1662	2	26	N/A	34.19 ^c	16.56	0.704	1.090

Table 3. continued

Lower Kittanning pyrolysis data with ~2% O ₂								
pressure (atm)	peak gas temp. (K)	collection height (in.)	residence time (ms)	mass release (daf wt %, ash tracer)	mass release (as rec'd wt %, direct)	ash (dry wt %)	apparent density ρ (g/cm ³)	swelling ratio d/d_0
pressure (atm)	0.84			5		10		15
heating rate (K/s)	1.03×10^5			1.03×10^5		1.25×10^5		1.11×10^5

^aExperiment performed in FFB rather than PFFB. ^bExperiment performed in FFB rather than PFFB, used average of direct and ash tracer mass release to calculate swelling. ^cUsed direct mass balance instead of ash tracer to calculate swelling.

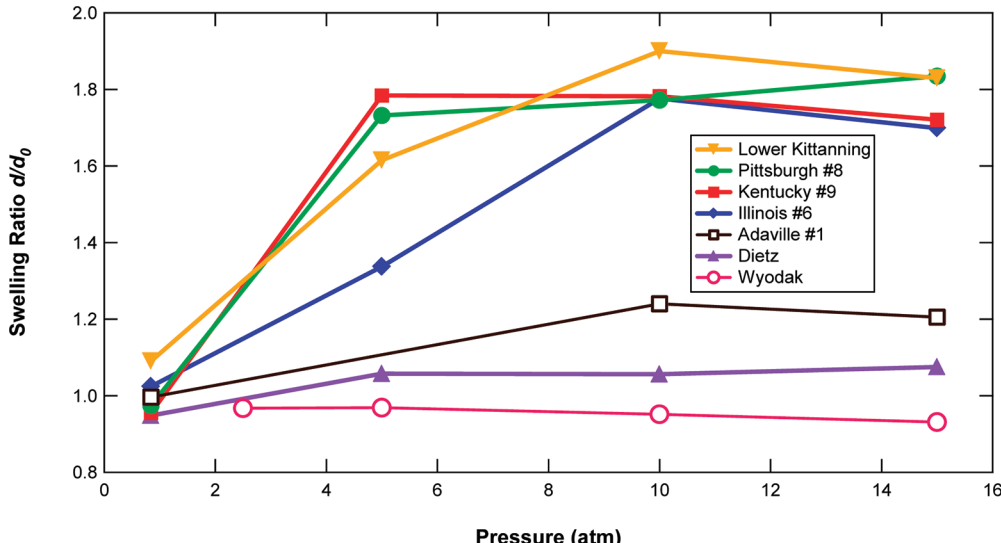


Figure 8. Swelling ratios with peak gas temperatures of 1700–1900 K and heating rates of $\sim 10^5$ K/s (see Table 3).

well-represented by the ASTM volatiles content. Most of the composition or coal rank dependence is included in the term s_{var} . The heating rate with the subscript “Base” is a reference heating rate with a value of 5.8×10^4 K/s.¹¹ The heating-rate dependence is fixed by the exponent c_{HR} which varies from zero for lignites and anthracites to near unity for many bituminous coals.

The pressure function $f(P)$ in eq 7 should have a value of unity at atmospheric pressure. The previous swelling model¹¹ can be extended to higher pressures by specifying the form of this pressure function and fitting parameters to pressurized pyrolysis data with well-defined heating rates in regime 2 (greater than $\sim 10^4$ K/s). The placement and form of the pressure dependence in this equation is critical, as can be seen by comparison to other swelling models. The most recent version of the CBK swelling correlation accounted for pressure effects by raising the atmospheric swelling ratio to a power that is a piecewise linear function of pressure.¹⁷ Previous atmospheric swelling experiments^{9,11} showed that bituminous coals can have swelling ratios with values below 1.0 at sufficiently high heating rates. If a formulation of pressure dependence similar to the CBK swelling model were to be used in this work, it would cause a physically unrealistic reduction in swelling with increasing pressure at high heating rates.

Extension of this swelling model to elevated pressures at low heating rates (below $\sim 8.5 \times 10^3$ K/s) is beyond the scope of this work. Extension of the model to subatmospheric pressures is also beyond the scope of this work. For application of this model, all ambient pressures can be assigned the value of 1 atm, regardless of the local value of absolute pressure. The consistency in the fit of the atmospheric data obtained in laboratories at elevations within 500 feet of sea level compared

to BYU data (0.84 atm at 4700 feet above sea level) support this approximation.^{11,19}

Equation 7 can be used to back-calculate the pressure factor $f(P)$ from experimental data if the heating rate is characterized carefully. This approach allows most of the effects of heating rate and some of the effects of coal type to be removed from the data so that the effects of pressure on swelling can be compared more directly between different coals and experimental conditions. The pressure factors obtained in this manner are sensitive to errors in the swelling ratio, the coal ultimate and proximate analyses, predicted NMR parameters, heating rates, and the correlations for s_{var} and c_{HR} .

When pressurized swelling data are reported, associated heating rates are often reported as identical (at least to 1 significant figure) for all pressures. If such reports are accurate (which in some cases is debatable) and one of the swelling ratios in the data set was obtained at atmospheric pressure, the pressure factor can be calculated from eq 7 as

$$f(P) = \frac{\left(\frac{d}{d_0}\right)_{P_2} - s_{\min}}{\left(\frac{d}{d_0}\right)_{P_1} - s_{\min}} \quad (9)$$

where the subscript P_2 indicates a char produced at high pressure and P_1 indicates a char produced at atmospheric pressure. This approach allows the effect of pressure on swelling to be determined, even if the correlations for s_{var} and c_{HR} are inaccurate for the coal in question. Equation 9 provides a convenient analysis approach in cases where the heating rates are believed to be nearly identical at all pressures investigated, but the numerical value of the heating rate is not available or

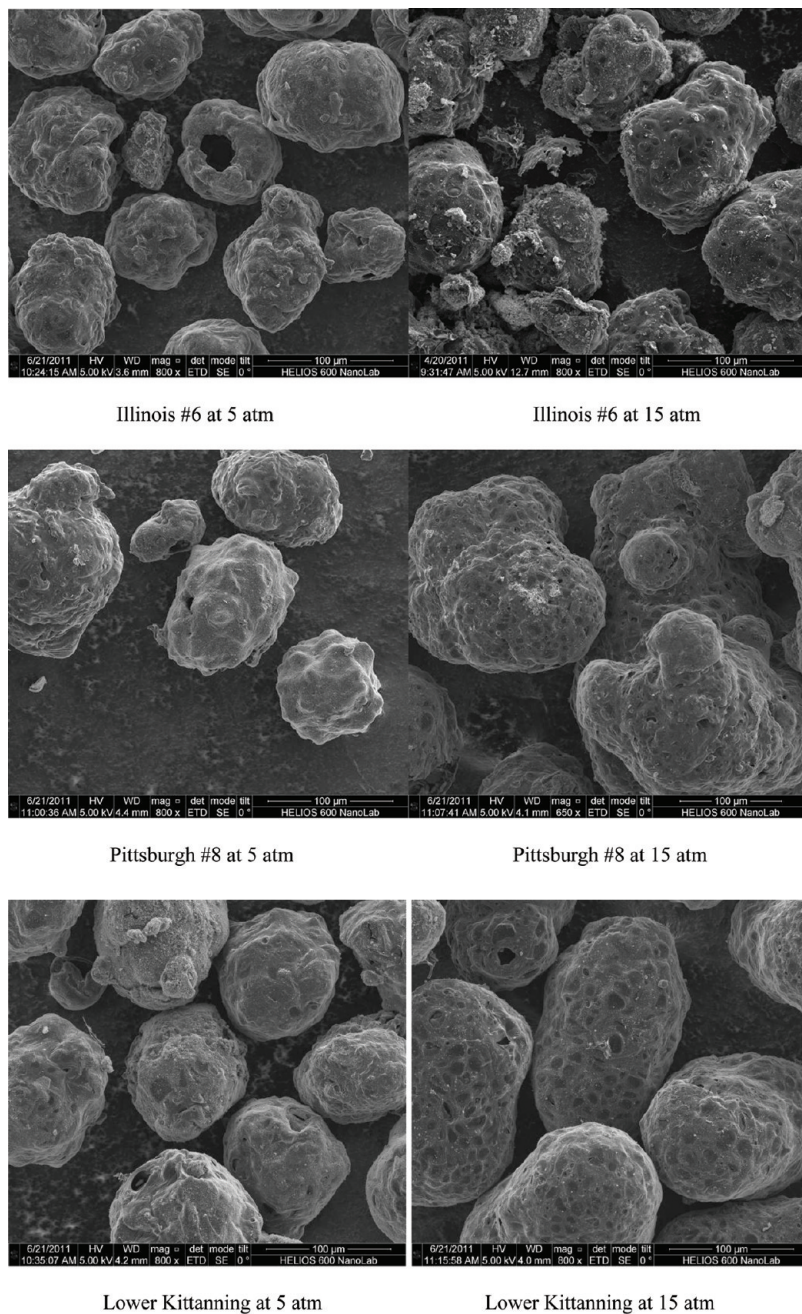


Figure 9. Bituminous chars produced at 5 and 15 atm in the PFFB.

calculated in a manner that is inconsistent with this work. If the coal of interest is well-represented by the model at atmospheric pressure, then the pressure factor can be calculated from eq 9 with the denominator (P_1) swelling ratio calculated from eq 7 at 1 atm.

When pressure factors are calculated for the data from previous studies presented in the literature review (see Figure 1) several trends become apparent (see Figure 11). Most significantly, the Illinois #6 data of Lee et al.³ at 10⁴ K/s no longer exceed the data with higher heating rates by a factor of 2–3. Rather, Lee's data are in good agreement with the Illinois #6 data of Zeng et al.²⁰ This result clearly demonstrates that the effect of heating rate is very important at elevated pressures. It appears that the relationship between heating rate and pressure

dependence used in this model formulation is a useful approximation.

The pressure factors in Figure 11 were calculated using the reported heating rates. The error bars were obtained by adjusting the heating rate to force the atmospheric pressure factor to have a value of 1. This scaling method is equivalent to using eq 9, and yields a reasonable estimate of a corrected heating rate when the coals are known to be well-represented by the atmospheric pressure model. The scaled heating rates and chemical structure information are listed in Table 4. It appears that the mechanistic model of Yu et al.⁵ yields behavior that is qualitatively in good agreement with the available data. This model has a maximum effect of pressure at about 8 atm, which could be viewed as a lower limit in consideration of other data that exhibit continued increases in swelling up to at least

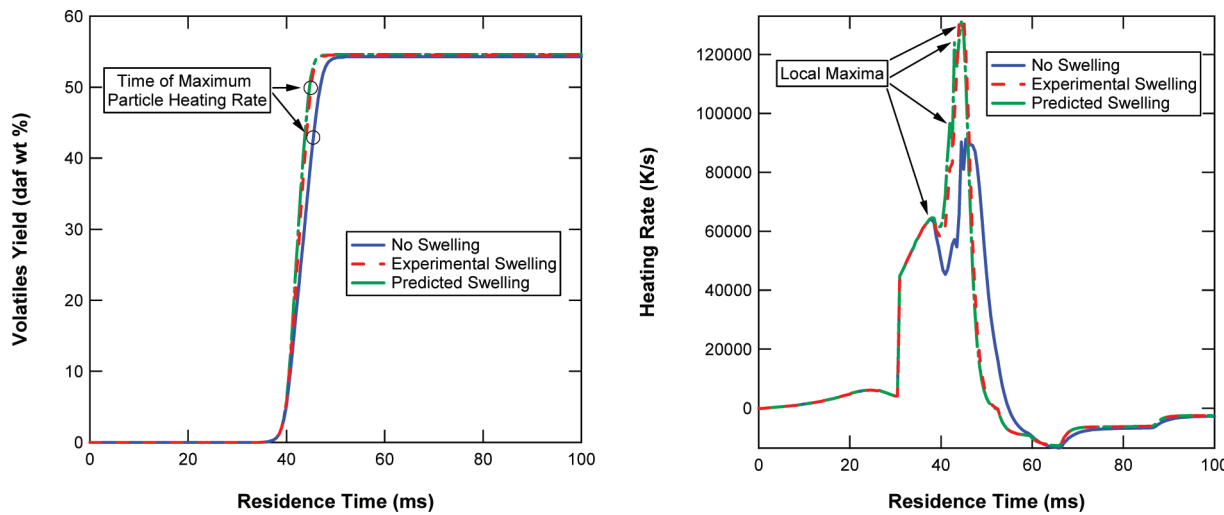


Figure 10. CPD predictions of volatiles yield and heating rate for Illinois #6 pyrolysis at 15 atm in the PFFB.

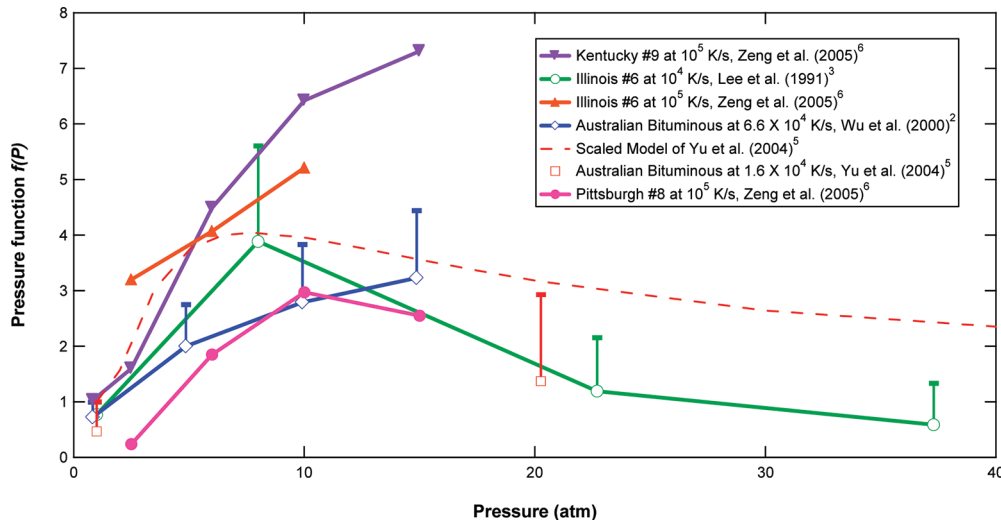


Figure 11. Effect of pressure on swelling for bituminous coals in previous studies.

Table 4. Heating Rates and Chemical Structure Information for Coals in Figure 11

coal	source	C/O	$(\sigma+1)$	M_δ	MW	reported HR, (K/s)	scaled HR (error bar), (K/s)
Kentucky #9	Zeng et al. ⁶	6.15	5.20	39.3	382.3	10^5	N/A
Illinois #6	Lee et al. ³	6.28	5.22	38.2	374.2	$\sim 10^4$	1.46×10^4
Illinois #6	Zeng et al. ⁶	7.37	5.27	37.0	380.4	10^5	N/A
Australian Bituminous	Wu et al. ²	9.44	4.84	28.6	308.5	6.6×10^4	9×10^4
Australian Bituminous	Yu et al. ⁵	9.73	4.84	30.4	344.5	1.6×10^4	3.52×10^4
Pittsburgh #8	Zeng et al. ⁶	11.4	4.80	29.0	344.9	10^5	N/A

15 atm (see Figure 11). However, it is possible that these apparent monotonic increases are caused by maximum particle heating rates that decrease as the pressure increases. In both this study and the data of Lee et al.,³ high heat loss at elevated pressures often resulted in decreasing heating rates with increasing pressure.

Heating rates of 10^4 K/s at 0.1 MPa and 7×10^3 K/s at 1.7 MPa were reported in the work of Lee et al.³ The pressure factors (Figure 11) for this data set were obtained by assuming that the heating rate was linear with the logarithm of pressure. The heating rates at 22.7 and 37.3 atm have extrapolated values of 6.1×10^3 K/s and 4.4×10^3 K/s, respectively. In the previous atmospheric swelling model,¹¹ the transition between

swelling regimes 1 and 2 was estimated to occur at a heating rate of 8.5×10^3 K/s (see Figure 3). If Lee's highest pressure data are in regime 1, the extrapolated regime 2 model (eq 7) would overestimate the effect of heating rate on swelling at these conditions. An overestimate of the effect of heating rate would result in pressure factors that are underestimated for the Illinois #6 data of Lee et al.³ at pressures above 8 atm (Figure 11).

The remaining data in the Figure 11 have a few anomalies, but there is also support for the formulation of this model. The Kentucky #9 data of Zeng et al.²⁰ include a swelling measurement at atmospheric pressure that is in excellent agreement with the model. However, the Pittsburgh #8 data

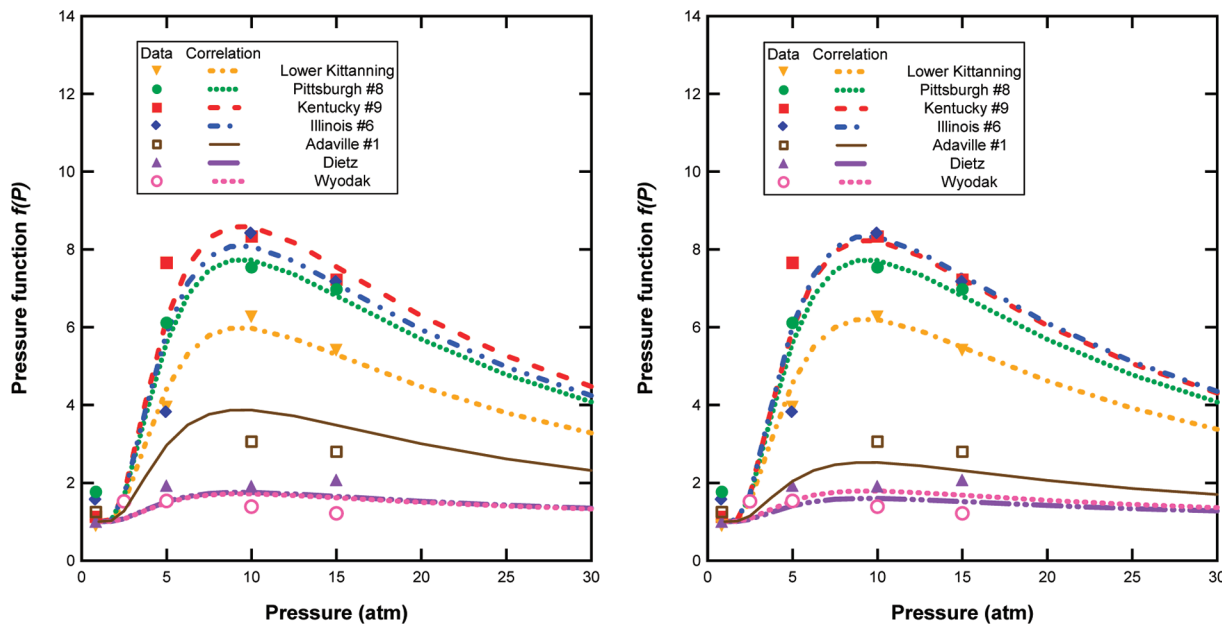


Figure 12. Pressure factors from PFFB and FFB data, including fits of c_{scale} versus $(\sigma+1)$ (left) and C/O (right) compared to experimental values.

Table 5. Scaling Factors for Pressure Function, Assuming $c_{\text{visc}} = 7.77$ and $c_{\text{ext}} = 3.47$

	Wyodak	Dietz	Adaville #1	Illinois #6	Kentucky #9	Pittsburgh #8	Lower Kittanning
c_{scale}	1.48	4.72	9.36	33.0	32.9	30.3	23.5

from the same publication appear to be too low at 2.5 atm; the pressure factor should not be less than 1. This could be due to some error in the measured coal properties, the swelling ratio, the calculated heating rate, or the correlations for s_{var} and c_{HR} . Errors in the correlations seem unlikely, since Pittsburgh #8 was in the training set for the previous model^{11,23} and has been shown to be well-represented by this model at atmospheric pressure (see Figure 3).^{9,11}

Scaling bars were not included for the Pittsburgh #8 series in Figure 11 because no atmospheric data were included in the publication.⁶ The pressure factors for the Pittsburgh #8 series could be scaled up until $f(2.5 \text{ atm}) > 1$ by adding a uniform offset or multiplying by some correction factor. Doing so would result in maximum pressure factors between 4 and 15 for Pittsburgh #8, which would yield a more reasonable trend for this highly swelling coal.

The high extent of overlap in the pressure factor error bars in Figure 11 makes it difficult to identify rank-dependence for swelling trends. However, the low effect of pressure on swelling for the Australian Bituminous coal of Wu et al.² compared to the other coals may be related to the low values of $(\sigma+1)$, M_δ and/or MW. This trend is particularly evident when this coal is compared to the Kentucky #9 data of Zeng et al.²⁰ (see Figure 11 and Table 4).

A mathematical form for the pressure function that can fit the observed behavior is

$$f(P) = 1 + \frac{c_{\text{scale}}[\ln(P)]^{c_{\text{visc}}}}{P^{c_{\text{ext}}}} \quad (10)$$

where the parameter c_{scale} determines the maximum magnitude of the effect of pressure. The parameter c_{visc} represents changes in viscoelastic properties of the Metaplast that allow increased swelling with increasing pressure. The parameter c_{ext} represents the extent to which the external pressure force restrains

swelling. This function has a derivative of zero at $P [\text{atm}] = 1$ and at $P_{\text{peak}} [\text{atm}] = \exp(c_{\text{visc}}/c_{\text{ext}})$. If c_{visc} is not an integer, this function is undefined below $P [\text{atm}] = 1$ because $\ln(P)$ is negative. Therefore, any ambient atmospheric pressure should be assigned the numerical value of 1 atm for application in this model.

The swelling data from Figure 8 are presented in terms of their pressure factors in Figure 12. The Lower Kittanning coal exhibits the smallest effect of pressure on swelling compared to the bituminous coals of lower ranks, even though the swelling ratios are very similar. This may indicate that the vapor pressure effect tends to optimize the Metaplast viscosity of bituminous coals to similar values. The subbituminous coals exhibit pressure factors close to 1. The clustering of the pressure factors at values near unity for the data at 0.84 atm indicates that these coals are represented reasonably well by the previously published atmospheric swelling model.¹¹ The curve fits using eq 10 shown in Figure 12 predict bituminous coal pressure functions with magnitudes between 2 and 4 at pressures of 40 to 60 atm. This is consistent with trends predicted by mechanistic bubble models.⁵ The trends at pressures typical of entrained-flow gasifiers are also consistent with the very limited data available at pressures above 20 atm (see Figure 11).

The curve-fits of the pressure factor shown in Figure 12 capture the trends of the data very well and were derived in a stepwise fashion. The steam coals Pittsburgh #8, Kentucky #9, and Illinois #6 have very similar pressure factors and are well-represented by the atmospheric model. The pressurized data from these three coals were fit to eq 10 with a single set of coefficients. Values of $c_{\text{visc}} = 7.77$ and $c_{\text{ext}} = 3.47$ were obtained, yielding $P_{\text{peak}} = 9.4$ atm, which is close to the lower limit of 8 atm suggested by previous data and models.^{3,5} These values for c_{visc} and c_{ext} were applied to all coals. This is equivalent to

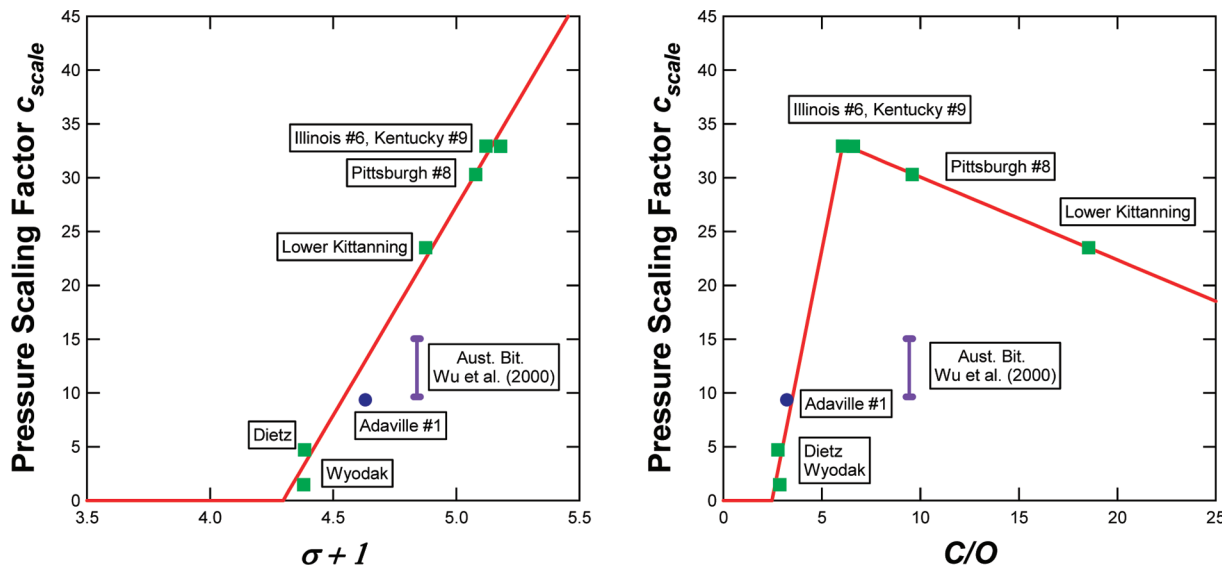


Figure 13. Correlations of c_{scale} versus coal rank.

assuming that all coals exhibit peak swelling at the same pressure.

The values of c_{scale} were then fit for each coal using only the data from 10 and 15 atm. The fitted c_{scale} values are shown in Table 5. Only the highest pressures were used to fit c_{scale} because the atmospheric data were irrelevant to the fit and the 5 atm data exhibited more scatter. This approach seemed reasonable because practical systems that include pressurized pyrolysis of particles smaller than $200\text{ }\mu\text{m}$ at heating rates above 10^4 K/s usually operate at pressures above 10 atm. It appears that maximum pressure factors of 7.5 to 8.5 for bituminous steam coals occur at pressures near 10 atm, which corresponds to c_{scale} values of 30 to 33 (see Table 5).

The values of the scaling factor c_{scale} were compared to various measures of coal chemical structure, as was done for other parameters in the development of the atmospheric swelling model.¹¹ The simplest fit of the parameter c_{scale} was linear with respect to $(\sigma+1)$ (see Figure 13), which initially increased with coal rank and then began to decrease at coal ranks slightly below high-volatile bituminous. The mass ratio C/O also gave reasonable results (see Figure 13), but only if a piecewise fit was used to account for differences in behavior between high-rank coals and low-rank coals.

The Adaville #1 coal experiments were performed as a follow-up to the other experiments. The Adaville #1 swelling data were not used to produce the fits shown in Figures 12 and 13. The $(\sigma+1)$ correlation over-predicted the c_{scale} value derived from the Adaville #1 swelling measurements by 3.6 units, and the C/O correlation under-predicted c_{scale} by 2.5 units. The agreement of the Adaville #1 with the C/O correlation is remarkably good considering that the splice point of the two-piece correlation was arbitrarily selected at the rank of Illinois #6 (see Figure 13). However, both fits of c_{scale} in Figure 13 show very reasonable agreement with the Adaville #1 coal when consideration is made for the small magnitude of the swelling measurements and the error associated with the swelling measurements, the heating rate, the ultimate and proximate analysis, and the other correlated coefficients in this swelling model. The Adaville #1 coal is borderline in rank between subbituminous and bituminous, and this correlation predicts that swelling does not depend on heating rate for this coal ($c_{HR} = 0$ in eq 7).¹¹

Experiments with different facilities or particle sizes would be required to determine whether the effect of heating rate is actually negligible for swelling of the Adaville #1 coal.

More experimental data would be required to confidently evaluate the performance of the c_{scale} correlations for the highest and lowest ranks of bituminous coals. Estimates of c_{scale} for an Australian bituminous coal² are shown in Figure 13 (see also Figures 1 and 11). These estimated c_{scale} values for the Australian bituminous coal depend on the reported heating rate and the other parameters in this swelling model, which means that the range of values shown in Figure 13 could be larger for this coal. The c_{scale} values derived from the data of Wu et al.² were more consistent with the $(\sigma+1)$ correlation compared to the C/O correlation. The trends of the other pressure factors derived from literature data (see Table 4 and Figure 11) mostly increase with increasing $(\sigma+1)$, but the trend is not as good for C/O. This suggests that the $(\sigma+1)$ correlation predicts more reasonable values for a greater variety of bituminous coals. The $(\sigma+1)$ correlation is therefore recommended generally, especially for bituminous coals, due to its simplicity and apparent robustness. However, the Adaville #1 data and the overall fit of the other coals studied in this work suggest that the C/O correlation yields slightly better predictions for many North American coals. Therefore, the C/O correlation is used for the remaining figures in this work.

The final pressure factors resulting from the $(\sigma+1)$ and C/O correlations (see Table 6) are compared to the experimental

Table 6. Correlations of c_{scale} for Use in the Pressure Function $f(P)$

	correlation	range of applicability	R^2
1 ^a	$c_{scale} = 38.89(\sigma + 1) - 167.1$	$\sigma + 1 \geq 4.297$	0.991
2a	$c_{scale} = -0.7704\left(\frac{C}{O}\right) + 37.77$	$6.04 \leq \frac{C}{O} \leq 49.0$	0.998
2b	$c_{scale} = 9.213\left(\frac{C}{O}\right) - 22.73$	$2.47 \leq \frac{C}{O} \leq 6.04$	0.986

^aCorrelation 1 is recommended for international coals due to its simplicity and robustness.

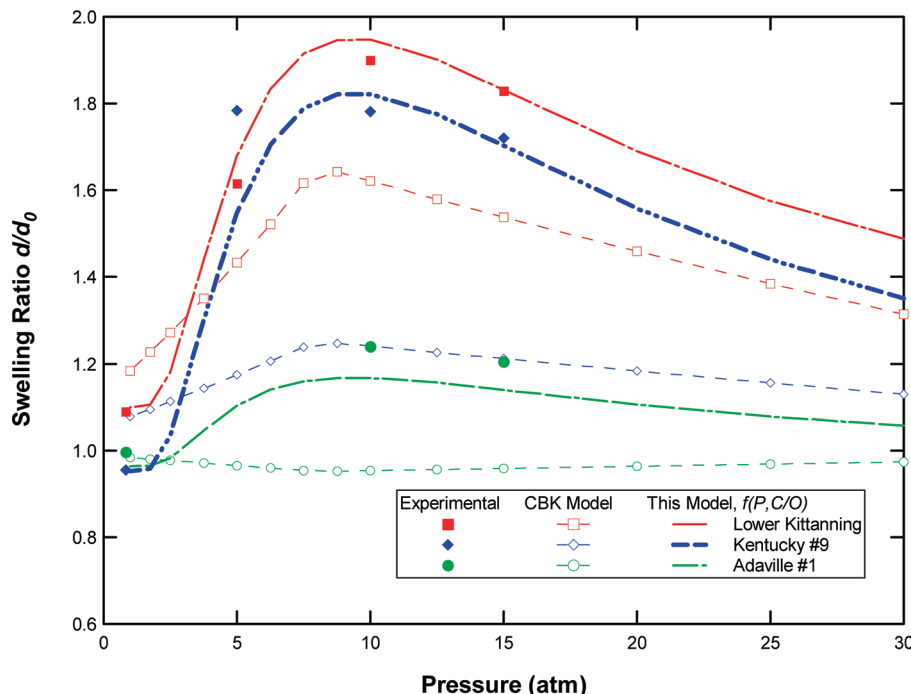


Figure 14. Experimental swelling ratios with the new pressurized swelling correlation and the CBK swelling correlation.^{16,17} Average heating rates of 1.13×10^5 K/s were assumed for Lower Kittanning and 1.29×10^5 K/s for Kentucky #9 based on the PFFB data.

values in Figure 12. The scatter in the pressure factors at 5 atm appear to result from the high slope of $f(P)$ at pyrolysis pressures below ~ 8 atm and the uncertainties in the calculated heating rate. Because of the structure of eq 7, moderate variations in the pressure factor do not have large effects on the swelling ratio, especially at heating rates higher than 10^5 K/s. If a value of 0.9 is assumed for s_{\min} with $d/d_0 - s_{\min} = 0.25$ at 1 atm, and the pressure factor has a range from 4 to 12 (typical for bituminous coal), changing the pressure factor by 1 unit changes the swelling ratio by 7–13%. Variations of 8–9% are obtained using a value of $d/d_0 - s_{\min} = 0.1$ with a pressure factor range from 1 to 4 (typical values for subbituminous coal). These projected variations in the predicted swelling ratio are comparable to the reported experimental error of 10% for the swelling ratio as determined by the tap density technique.²⁴

A comparison of experimental and predicted swelling ratios for three of the coals in this study is shown in Figure 14. Swelling ratios predicted from the CBK swelling correlation^{16,17} are also shown for the same coals (curves with open symbols). The CBK swelling correlation has no heating rate dependence and hence performs very poorly for the coals shown in Figure 14 compared to the new pressurized swelling model. It has been shown previously¹¹ that this model also matches atmospheric pressure swelling data better than the CBK swelling correlation, which is a result of the form of eq 7 and the coal rank dependence included in its parameters, especially s_{var} .

The curves without symbols in Figure 14 were produced using the C/O correlations in Table 6 and average heating rates from the pressurized experimental data. Adaville #1 had zero predicted heating rate dependence (c_{HR}) in this model due to its low rank.¹¹ The correlated swelling ratios using the C/O correlations in Table 6 deviated from the experimental measurements at 10 atm by only 2% for Kentucky #9 and Lower Kittanning, which are at nearly opposite ends of the highly swelling bituminous rank spectrum (see Figure 13).

With the $(\sigma+1)$ correlation from Table 6, the deviations from experimental values for the same coals at 10 atm are 5% and 0.6%, respectively. The predicted swelling ratio using the C/O correlation at 10 atm for the Adaville #1 coal deviated from the experimental value by 6%, compared to 9% for the $(\sigma+1)$ correlation. The two versions of the new swelling model actually bracket the pressurized experimental values for Adaville #1. The agreement of both versions of the model with the Adaville #1 data is quite reasonable, especially considering the difficulty of capturing the transition from subbituminous shrinkage to bituminous swelling and all the possible sources of error to the experimental swelling data and the inputs to the swelling model.

The Australian bituminous data of Wu et al.² had an effect of pressure on swelling that was smaller than most other bituminous coals in the literature (see Figure 13). Southern hemisphere coals are petrographically different from northern hemisphere coals, with higher concentrations of inertinite in southern hemisphere coals. For this reason, studies that include southern hemisphere coals often correlate pyrolysis and combustion properties with vitrinite and inertinite concentrations rather than the more convenient ultimate and proximate analyses.^{29,36,37} Heating rates would need to be calculated with methods identical to this work to determine how well this swelling model performs for southern hemisphere coals. However, it appears that the NMR parameters predicted from correlations²⁶ with the ultimate and proximate analyses yield reasonable swelling trends for the data of Wu et al.² (see Figure 13). Vitrinite and inertinite contents have also been correlated with carbon and hydrogen content,³⁸ which may explain why the use of chemical structure features derived from elemental analysis might yield good predictive results for Southern Hemisphere coals.

A parity plot comparing the new swelling model to the pressure-dependent pyrolysis swelling data from this study is shown in Figure 15. The Adaville #1 data are plotted separately

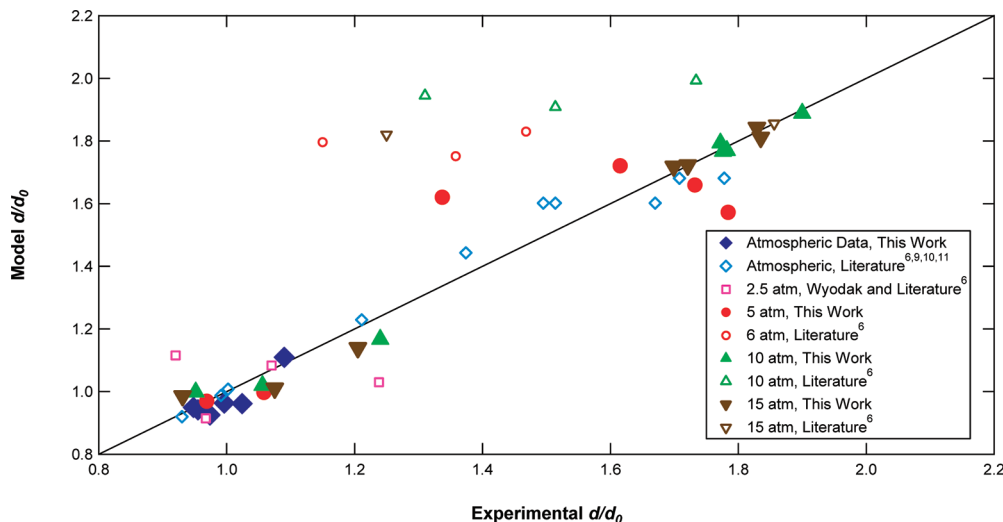


Figure 15. Parity plot of new swelling correlation using the C/O pressure function. Solid symbols represent data from this work, open symbols from the literature. Zeng et al.⁶ reported only one significant figure for the maximum particle heating rate.

from the bituminous and subbituminous training sets that were used to develop the correlations for the pressure functions. The C/O version of the correlation is shown due to the slightly better fit of the training set and the Adaville #1. The high-heating rate atmospheric data from Figure 3 are also shown, as well as the pressurized data of Zeng et al.⁶ It is likely that the poor agreement with much of the data of Zeng et al. is due to the fact that the heating rate was reported as simply 10^5 K/s⁶ and also because the Pittsburgh #8 swelling data of Zeng et al. seem unreasonably low (see Figure 11 and associated commentary). This swelling model requires a carefully calculated maximum particle heating rate that is reported to ~ 3 significant figures. This is especially important at heating rates below 10^5 K/s, as can be seen by inspecting Figure 3. The low number of significant figures reported at heating rates on the order of 10^4 K/s for the data of Lee et al.,³ Wu et al.,² and Yu et al.⁵ shown in Figures 1 and 11 made quantitative predictions with the new model impractical. The reported swelling ratios in these drop tube studies occurred in a region of such high variation of swelling with heating rate (see Figure 3) that the use of only 1 or 2 significant figures can result in very large errors at elevated pressures. The model predicts swelling ratios for the data of Wu et al.² that are near 2.5 compared to experimental values near 1.5. However, for the data of Yu et al.⁵ and Lee et al.,³ the model yields swelling ratios between 5 and 6 when the experimental values were near 2. For the maximum swelling ratio of Lee et al.,³ (nearly 4, see Figure 1) the model yields a predicted value slightly lower than 7. Figure 11 shows estimates of how much heating rate can affect the perceived effect of pressure for these coals. For this swelling model to be applied correctly, it is critical to calculate the particle temperature history in a careful manner that is consistent with this study and report the maximum particle heating rate as defined in eq 2 and shown in Figure 10. Use of average heating rate or other definitions or estimates of the heating rate do not work well with this model.

Most of the scatter in Figure 15 occurs at 5 atm. This is caused by the sparse data at pressures in the vicinity of maximum swelling and the simplifying assumptions used to fit the coefficients in eq 10. The 5 atm data were used to help define an average shape of the pressure function via c_{visc} and c_{ext} and hence the pressure corresponding to maximum swelling

(9.4 atm). Only the data at 10 and 15 atm were used to fit the final version of $f(P)$ via c_{scale} . Hence, the new pressurized swelling model performs best at pressures above 10 atm, where swelling gradually decreases with increasing pressure. Pulverized-coal gasifiers generally operate in this regime of pressure. This model can probably be upgraded to yield better predictions of maximum swelling if data become available for a variety of coals at smaller pressure increments in the vicinity of maximum swelling (below 10 atm).

5. CONCLUSIONS

Pressurized coal pyrolysis experiments confirmed that the maximum magnitude of the swelling ratio is usually less than 2 at heating rates of $\sim 10^5$ K/s. Swelling initially increased rapidly with increasing pressure for bituminous coals. Very similar swelling ratios were observed for several different bituminous coals. Little or no swelling occurred for subbituminous coals, even at elevated pressures. These data expand and clarify knowledge of swelling trends with pressure and coal rank. Maximum swelling appears to occur for most coals in the vicinity of 10 atm, and most of the increase in swelling appears to occur below 5 atm. Some of the data suggest that swelling continues to increase for some coals at pressures of at least 15 atm. However, other data show little change from 5 to 15 atm, suggesting that moderate decreases in the particle heating rate with increasing pressure could cause the apparent monotonic increase in swelling.

A new swelling model has been developed that allows the effects of pressure on coal swelling to be separated from the effects of heating rate. This pressure factor approach was used to largely eliminate the differences observed in the effect of pressure on swelling ratios measured at different heating rates in drop-tube furnaces and flat-flame burners. The new pressurized swelling data were used to correlate the effect of pressure with the chemical structure of the coal. It was found that several of the bituminous steam coals have very similar pressure factors. The new swelling model works best when the maximum particle heating rate is computed rather than using an average or estimated particle heating rate.

AUTHOR INFORMATION

Corresponding Author

*Email: tom_fletcher@byu.edu.

Notes

The authors declare no competing financial interest.

ACKNOWLEDGMENTS

This material is based upon work supported by the Department of Energy under Award Number DE-NT0005015. The views and opinions of authors expressed herein do not necessarily state or reflect those of the United States Government or any agency thereof.

NOMENCLATURE

- A = ash fraction (from ASTM proximate analysis, dry basis), surface area (m^2)
- B = mass flux term in the blowing parameter
- CPD = chemical percolation devolatilization model
- c_{HR} = coefficient in swelling correlation relating to heating rate
- c_p = constant pressure specific heat of solid particle ($\text{J}/\text{kg K}$)
- \hat{c}_{pg} = constant pressure specific heat of gas around particle ($\text{J}/\text{kg K}$)
- c_{scale} = coefficient in swelling correlation used to scale the effect of pressure
- c_{ext} = coefficient in swelling correlation related to restrained swelling at very high pressures
- c_{visc} = coefficient in swelling correlation related to changes in viscoelastic properties of coal
- d = diameter (m)
- d/d_0 = swelling ratio
- $f(P)$ = function defining effect of pressure on swelling
- FC = fixed carbon fraction (from ASTM proximate analysis, dry basis)
- FFB = flat-flame burner
- h = convective heat transfer coefficient (m^2/s)
- HR = Heating rate
- k_g = thermal conductivity ($\text{W}/(\text{m K})$)
- L = labile bridge fraction from CPD model
- m = mass (kg)
- M_δ = mass per side chain (from ^{13}C NMR data)
- P = pyrolysis pressure (atm)
- P_1 = atmospheric pressure (1 atm)
- P_2 = elevated pressure (atm)
- PFFB = pressurized flat-flame burner
- swell = fractional swelling parameter defined as $d/d_0 - 1$
- $s_{\text{var.}}$ = coefficient in swelling correlation relating to coal structure
- s_{min} = coefficient in swelling correlation relating to minimum size
- t = time (s)
- T = temperature (K)
- \dot{T} = heating rate (K/s)
- TGA = thermogravimetric analyzer
- VM = volatile matter fraction (from ASTM proximate analysis, dry, ash-free basis)
- WMR = wire mesh reactor
- ΔH = change in enthalpy due to reaction and vaporization (J/kg)
- ϵ = packing factor, emissivity
- ρ = density (kg/m^3)
- σ = Stefan–Boltzmann constant = $5.67 \times 10^{-8} \text{ W}/(\text{m}^2 \text{ K}^4)$

$\sigma+1$ = coordination number (attachments per cluster) from ^{13}C NMR data

θ = blowing factor (dimensionless)

Subscripts

ASTM = from ASTM proximate analysis

b = bulk or bed

Base = baseline condition

g = gas

HHR = high heating rate ($>8.5 \times 10^3 \text{ K/s}$)

max = maximum

min = minimum

p = particle

surr = surrounding surfaces

0 = initial

REFERENCES

- (1) Solomon, P. R.; Fletcher, T. H. Impact of Coal Pyrolysis on Combustion. *Symp. (Int.) on Combust., [Proc.]* **1994**, *25*, 463–74.
- (2) Wu, H.; Bryant, G.; Benfell, K.; Wall, T. An Experimental Study on the Effect of System Pressure on Char Structure of an Australian Bituminous Coal. *Energy Fuels* **2000**, *14* (2), 282–290.
- (3) Lee, C. W.; Scaroni, A. W.; Jenkins, R. G. Effect of Pressure on the Devolatilization and Swelling Behavior of a Softening Coal During Rapid Heating. *Fuel* **1991**, *70* (8), 957–965.
- (4) Yu, J.; Harris, D.; Lucas, J.; Roberts, D.; Wu, H.; Wall, T. Effect of Pressure on Char Formation during Pyrolysis of Pulverized Coal. *Energy Fuels* **2004**, *18* (5), 1346–1353.
- (5) Yu, J.; Lucas, J.; Wall, T.; Liu, G.; Sheng, C. Modeling the Development of Char Structure During the Rapid Heating of Pulverized Coal. *Combust. Flame* **2004**, *136* (4), 519–532.
- (6) Zeng, D.; Clark, M.; Gunderson, T.; Hecker, W. C.; Fletcher, T. H. Swelling Properties and Intrinsic Reactivities of Coal Chars Produced at Elevated Pressures and High Heating Rates. *Proc. Combust. Inst.* **2005**, *30* (2), 2213–2221.
- (7) Goetz, G. J.; Nsakala, N. Y.; Patel, R. L.; Lao, T. C. Combustion and Gasification Kinetics of Chars from Four Commercially Significant Coals of Varying Rank. *Second Annual Contractors' Conference on Coal Gasification*, Palo Alto, CA, Oct. 20–21, 1982.
- (8) Hurt, R.; Sun, J.-K.; Lunden, M. A Kinetic Model of Carbon Burnout in Pulverized Coal Combustion. *Combust. Flame* **1998**, *113* (1–2), 181–197.
- (9) Gale, T. K.; Bartholomew, C. H.; Fletcher, T. H. Decreases in the Swelling and Porosity of Bituminous Coals during Devolatilization at High Heating Rates. *Combust. Flame* **1995**, *100* (1–2), 94–100.
- (10) Eiteneer, B.; Subramanian, R.; Maghzi, S.; Zeng, C.; Guo, X.; Long, Y.; Chen, L.; JS, R.; Raman, A.; Jain, J.; Fletcher, T.; Shurtz, R. Gasification Kinetics: Modeling Tools Development and Validation, *26th Annual International Pittsburgh Coal Conference*, Pittsburgh, PA, 2009.
- (11) Shurtz, R. C.; Kolste, K. K.; Fletcher, T. H. Coal Swelling Model for High Heating Rate Pyrolysis Applications. *Energy Fuels* **2011**, *25* (5), 2163–2173.
- (12) Oh, M. S.; Peters, W. A.; Howard, J. B. An Experimental and Modeling Study of Softening Coal Pyrolysis. *AIChE J.* **1989**, *35* (5), 775–792.
- (13) Sheng, C. D.; Azevedo, J. L. T. Modeling the Evolution of Particle Morphology During Coal Devolatilization. *Proc. Combust. Inst.* **2000**, *28* (2), 2225–2232.
- (14) Melia, P. F.; Bowman, C. T. A Three-Zone Model for Coal Particle Swelling. *Combust. Sci. Technol.* **1983**, *31* (3–4), 195–201.
- (15) Kidena, K.; Yamashita, T.; Akimoto, A. Prediction of Thermal Swelling Behavior on Rapid Heating Using Basic Analytical Data. *Energy Fuels* **2007**, *21* (2), 1038–1041.
- (16) Sun, J. K.; Hurt, R. H.; Niksa, S.; Muzio, L.; Mehta, A.; Stallings, J. A Simple Numerical Model to Estimate the Effect of Coal Selection on Pulverized Fuel Burnout. *Combust. Sci. Technol.* **2003**, *175* (6), 1085–1108.

- (17) Niksa, S.; Liu, G. S.; Hurt, R. H. Coal Conversion Submodels for Design Applications at Elevated Pressures. Part I. Devolatilization and Char Oxidation. *Prog. Energy Combust. Sci.* **2003**, *29* (5), 425–477.
- (18) Zygourakis, K. Effect of Pyrolysis Conditions on the Macropore Structure of Coal-Derived Chars. *Energy Fuels* **1993**, *7* (1), 33–41.
- (19) Shurtz, R. C. Effects of Pressure on the Properties of Coal Char Under Gasification Conditions at High Initial Heating Rates. Ph.D. Dissertation, Chemical Engineering Department, Brigham Young University, Provo, UT, 2011.
- (20) Zeng, D.; Fletcher, T. H. Effects of Pressure on Coal Pyrolysis and Char Morphology. *Energy Fuels* **2005**, *19* (5), 1828–1838.
- (21) Ma, J.; Fletcher, T. H.; Webb, B. W. Effect of Flame Environment on Soot Formation in Coal Combustion. *Coal Sci. Technol.* **1995**, *24*, 869–72.
- (22) Solum, M. S.; Sarofim, A. F.; Pugmire, R. J.; Fletcher, T. H.; Zhang, H. ^{13}C NMR Analysis of Soot Produced from Model Compounds and a Coal. *Energy Fuels* **2001**, *15* (4), 961–971.
- (23) Fletcher, T. H. Swelling Properties of Coal Chars during Rapid Pyrolysis and Combustion. *Fuel* **1993**, *72* (11), 1485–95.
- (24) Tsai, C.-Y.; Scaroni, A. W. The Structural Changes of Bituminous Coal Particles During the Initial Stages of Pulverized-Coal Combustion. *Fuel* **1987**, *66*, 200–206.
- (25) Zhang, H. Nitrogen Evolution and Soot Formation during Secondary Coal Pyrolysis. Ph.D. Dissertation, Chemical Engineering, Brigham Young University, Provo, UT, 2001.
- (26) Genetti, D.; Fletcher, T. H.; Pugmire, R. J. Development and Application of a Correlation of ^{13}C NMR Chemical Structural Analyses of Coal Based on Elemental Composition and Volatile Matter Content. *Energy Fuels* **1999**, *13* (1), 60–68.
- (27) Fletcher, T. H.; Kerstein, A. R.; Pugmire, R. J.; Solum, M. S.; Grant, D. M. Chemical Percolation Model for Devolatilization. 3. Direct Use of ^{13}C NMR Data to Predict Effects of Coal Type. *Energy Fuels* **1992**, *6* (4), 414–31.
- (28) Fletcher, T. H. CPDCP_NLG Code. <http://www.et.byu.edu/~tom/cpd/cpcodes.html> (accessed: May 10, 2012)
- (29) Yu, J.; Lucas, J. A.; Wall, T. F. Formation of the Structure of Chars during Devolatilization of Pulverized Coal and its Thermoproperties: A Review. *Prog. Energy Combust. Sci.* **2007**, *33* (2), 135–170.
- (30) Fletcher, T. H. Time-Resolved Temperature Measurements of Individual Coal Particles during Devolatilization. *Combust. Sci. Technol.* **1989**, *63* (1–3), 89–105.
- (31) Bird, R. B.; Stewart, W. E.; Lightfoot, E. N., *Transport Phenomena*. 2 ed.; John Wiley & Sons: New York, 2002.
- (32) Spalding, D. B. *Some Fundamentals of Combustion*; Butterworths Scientific Publications: London, 1955.
- (33) Merrick, D. Mathematical Models of the Thermal Decomposition of Coal: 2. Specific Heats and Heats of Reaction. *Fuel* **1983**, *62* (5), 540–546.
- (34) Maloney, D. J.; Sampath, R.; Zondlo, J. W. Heat Capacity and Thermal Conductivity Considerations for Coal Particles During Early Stages of Rapid Heating. *Combust. Flame* **1999**, *116*, 94–104.
- (35) Smoot, L. D.; Pratt, D. T. *Pulverized Coal Combustion and Gasification*; Plenum Press: New York, 1979.
- (36) Benfell, K. E.; Liu, G. S.; Roberts, D. G.; Harris, D. J.; Lucas, J. A.; Bailey, J. G.; Wall, T. F. Modeling Char Combustion: The Influence of Parent Coal Petrography and Pyrolysis Pressure on the Structure and Intrinsic Reactivity of Its Char. *Proc. Combust. Inst.* **2000**, *28*, 2233–2241.
- (37) Falcon, R.; Ham, A. J. The Characteristics of Southern African Coals. *J. South Afr. Inst. Min. Metall.* **1988**, *88* (5), 145–161.
- (38) Tang, L. G.; Gupta, R. P.; Sheng, C. D.; Wall, T. F. A Mechanistic Approach To Characterize Coal Heterogeneity in Predicting High-Temperature Volatile Matter Yields. *Energy Fuels* **2004**, *18* (6), 1716–1722.